Research Article Vol. 12, No. 10 / 1 Oct 2021 / Biomedical Optics Express 6269

Biomedical Optics EXPRESS

Femtosecond diode-based time lens laser for multiphoton microscopy

Y. Lange Simmons,[1] Kenneth J. Underwood,[1] Omkar D. Supekar,[2,3] Brendan M. Heffernan,[1] Tarah A. Welton,[4] Emily A. Gibson,[4] and Juliet T. Gopinath[1,3,*]

[1] Department of Physics, University of Colorado, Boulder, CO 80309, USA
[2] Department of Mechanical Engineering, University of Colorado, Boulder, CO 80309, USA
[3] Department of Electrical, Computer, and Energy Engineering, University of Colorado, Boulder, CO 80309, USA
[4] Department of Bioengineering, University of Colorado Anschutz Medical Campus, Aurora, CO 80045, USA
[*] Juliet.Gopinath@colorado.edu

Abstract: We demonstrate a near-infrared, femtosecond, diode laser-based source with kW peak power for two-photon microscopy. At a wavelength of 976 nm, the system produces sub-ps pulses operating at a repetition rate of 10 MHz with kilowatt class peak powers suitable for deep tissue two-photon microscopy. The system, integrated with a laser-scanning microscope, images to a depth of 900 µm in a fixed sample of PLP-eGFP labeled mouse brain tissue. This represents a significant development that will lead to more efficient, compact, and accessible laser sources for biomedical imaging.

© 2021 Optical Society of America under the terms of the OSA Open Access Publishing Agreement

1. Introduction

Pulsed lasers in the near-infrared find use in groundbreaking scientific and medical research, including biological imaging [1,2], laser surgery [3], and the study of Alzheimer's and Parkinson's disease [4–6]. Chief among these is their ability to probe the structure, function, and activity of neurons through multiphoton microscopy, including real-time monitoring and control of neuronal activity [1,2]. In conjunction with genetically encoded indicators such as GCaMP and GFP (two-photon absorption peaking around 976 nm), these lasers enable imaging of biological tissue up to millimeter depths [7–9]. Multiphoton imaging possesses distinct advantages over its single-photon excitation counterpart. The square dependence (two-photon) on intensity for excitation provides intrinsic axial sectioning [7,10]. The longer wavelength light reduces Rayleigh scattering, allowing greater imaging depths, and is spectrally separated from the emission light [10,11]. Sources suitable for multiphoton imaging must produce a high photon flux for multiphoton excitation, achieved with high peak power, sub-ps pulses [7]. With the numerous, impactful applications of multiphoton microscopy, we seek to improve near-infrared pulsed sources to create wider adoption and lower the barrier for use of multiphoton technologies.

Ultrafast pulsed lasers in the near-infrared (near-IR), have numerous drawbacks that complicate their use. The most popular sources, Ti:Sapphire lasers, often in conjunction with optical parametric oscillators (OPO), are prohibitively expensive, inefficient, and have large footprints. There are also mode-locked fiber ring oscillators that operate at 920 nm and 976 nm; however these have fixed repetition rates and require pulse picking for further adjustment [12,13]. In contrast, diode lasers provide an attractive solution. They are one of the most widespread and successful laser technologies, and are compact, inexpensive and power efficient. We demonstrate a viable path forward with a diode-based source that has comparable performance to popular sources for multiphoton imaging with a design including pulse shaping and enhancement techniques [14].

#430549 https://doi.org/10.1364/BOE.430549
Journal © 2021 Received 5 May 2021; revised 30 Jul 2021; accepted 20 Aug 2021; published 14 Sep 2021

Biomedical Optics EXPRESS

While diode lasers are low cost, compact and robust, there are issues that arise in pulsed operation. The fundamental physics—short upper-state lifetime and large two-photon absorption—of the semiconductor gain media limits achievable pulse energy and peak power [15–19]. We set out to overcome these limitations with a novel approach combining external pulse shaping, fiber amplification, and nonlinear pulse compression to greatly outperform other diode-based systems.

We chose to employ several pulse enhancement techniques in concert to achieve excellent performance from a pulsed laser diode. This novel approach to pulse generation allows us to maintain the benefits of each individual approach and achieve better results than with any one alone. We use a "time lens" paired with fiber amplification, similar to chirped-pulse amplification, to increase pulse energy and decrease pulse duration in tandem [20–22]. For further enhancement, double clad fiber amplification and compression of chirped pulses are used to further increase peak pulse power [23]. Research on ultrafast diode lasers report impressive results [24–26], but have not covered the wavelength range needed for two-photon microscopy with GFP [27]. The resulting performance of system presented here offers a path towards low cost, miniaturizable, and robust systems for biomedical research and clinical applications.

Our laser produces kilowatt peak power femtosecond pulses in the near-infrared, a critical region for multiphoton microscopy, by overcoming drawbacks in diode lasers that traditionally prohibit high peak powers. In this work, we report on a diode-based laser system with a tunable repetition rate. The source has an optimized repetition rate and wavelength for multiphoton imaging of the brain and peripheral nerves. The wavelength of the laser, 976 nm, is near the peak for two-photon response of eGFP, GCaMP, and YFP (requiring labeling or genetic modification) [27]. Additionally, it is also a suitable pump wavelength for coherent anti-Stokes Raman Scattering (CARS) microscopy (a label-free process) [28,29]. Further, we validate the laser for multiphoton microscopy by imaging fixed brain samples of PLP-eGFP mice [30]. We demonstrate fluorescent imaging at depths of 900 μm in the neo-cortex.

2. Laser design

Our laser consists of five stages: a pulsed diode seed, amplitude and phase control, amplification, spectral broadening, and a compressor (Fig. 1). Generation of clean seed pulses is critical to avoid amplifying a continuous wave (CW) signal. To achieve a high extinction ratio between the pulse and background, a combination of diode gain switching and amplitude modulation is used. A 976 nm distributed Bragg reflector (DBR) laser diode (Photodigm PH976DBR180BF) is electronically pumped with a high repetition rate, short pulse laser driver (Highland Technology T165), producing optical pulses with a full-width at half-maximum (FWHM) of approximately 70 ps and 200 mW peak power. A distributed Bragg reflector diode was chosen for its ability to produce short, stable pulses in this regime, enabled by the shorter cavity length when compared to other diode lasers [31]. The repetition rate is electronically controlled and can be adjusted from 1 MHz to 200 MHz, which allows for balancing peak and average powers for optimal imaging conditions [32,33]. To avoid photobleaching of samples and to maximize fluorescence signal while maintaining high frame acquisition rates, an operating repetition rate of 10 MHz was chosen [33].

In the second of the four stages, as seen in Fig. 1, the seed pulses are amplitude modulated with an electro-optic modulator (EOM, EOSPACE AZ-0S5-20-PFA-PFA-980) to shorten the width of gain switched pulse and match the profile of the phase modulation in the next step. The EOM is operated at 18 GHz to carve out an approximately 20 ps from the pulse envelope, with ~20 dB of extinction. This results in a small satellite pulse as the gain switched pulse width is greater than the wavelength of the 18 GHz modulation signal. These pulses are phase modulated with an electro-optic phase modulator (EOSPACE, PM-DS5-20-PFA-PFA-980-LV) also driven at 18 GHz with 30 dBm ($V_\pi < 3$ V, ~10 radians maximum). This phase modulation is the first step of the time lens system, adding a quadratic phase to the pulse.

Biomedical Optics EXPRESS

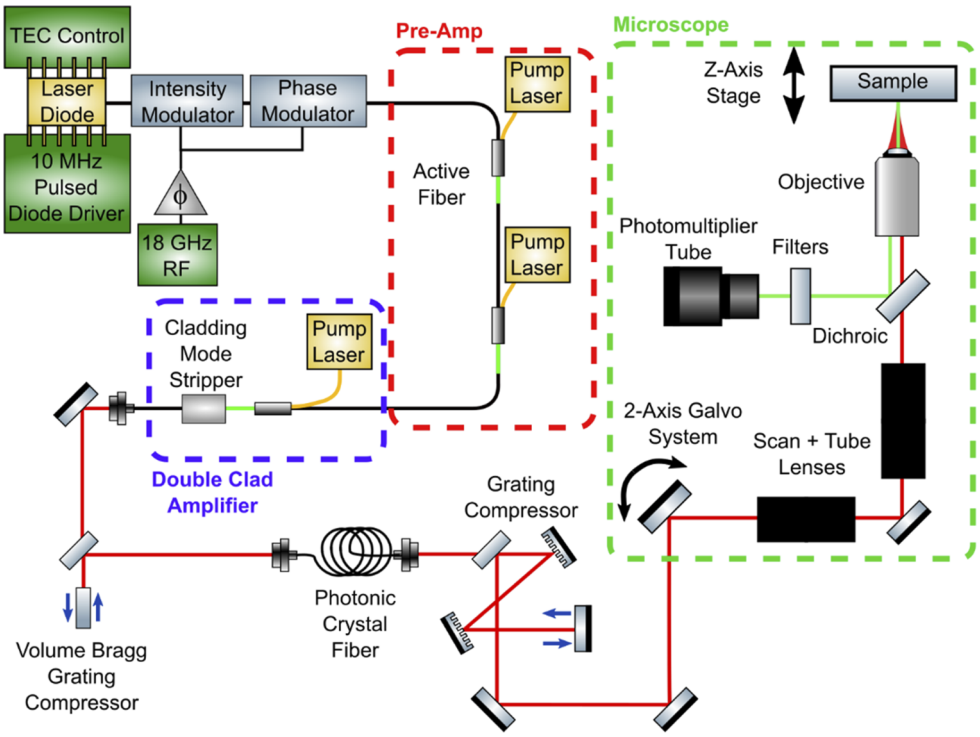

Fig. 1. Diagram of laser system. Pulses from a gain-switched diode are sent through amplitude and phase modulators, which have a controllable delay offset. Two stages of single mode fiber amplification with 976 nm notch filters to remove pump light make up the pre-amplification. The power amplification stage consists of a double-clad amplifier and a cladding mode stripper. A chirped volume Bragg grating (VBG) compresses the time lens pulses. Pulses are further compressed through self-phase modulation in photonic crystal fiber and a grating pair compressor.

After modulation, the pulses go through a multi-stage amplifier, consisting of two stages of Yb-doped single mode fiber amplification to scale the system average power followed by a Yb-doped double-clad fiber final amplification stage. The single mode amplifiers use 180 mW and 300 mW of 915 nm light to pump 10 cm and 16 cm fiber lengths (CorActive Yb401), respectively, achieving 56 mW average power [21]. Further amplification to 250 mW is achieved with double clad Yb-doped fiber (46 cm, LIEKKI Yb1200-10/125DC) cladding pumped at 40 W. This fiber length and large pump power are to help overcome the overlap of the absorption and emission cross sections at 976 nm and strong ASE that hinders Yb fiber amplification around 980 nm [34,35]. Excess pump light is removed with a cladding mode stripper (DK Photonics CPS-30-50-10/125/008/046-10). Pulses are coupled out of the fiber and compressed using a chirped volume Bragg grating (OptiGrate CBG-976-85, AR coated, 85% diffraction efficiency), which induces 17 ps/nm of dispersion, completing the time lens. Autocorrelations after compression show the pulses to be 2 ps FWHM with an average power of 180 mW, which match simulated results (Fig. S1).

These pulses are further temporally compressed through self-phase modulation in fiber and dispersion compensation. The pulses are coupled into single mode silica fiber (Corning HI1060) from free space after the volume Bragg grating. The silica fiber is spliced to photonic crystal fiber (PCF) (NKT SC-5.0-1040, mode field diameter 4 μm, -1.2 dB splice loss) which offers

Biomedical Optics EXPRESS

an increased effective nonlinear coefficient (11 $W^{-1}km^{-1}$ vs. 5 $W^{-1}km^{-1}$) due to its smaller mode field diameter (4 μm) compared to other single mode fibers (Corning HI 1060, mode field diameter 6 μm). Combined input and output coupling losses as well as splice loss total -2.2 dB. The spectrally broadened pulses are collimated and compressed with a grating pair, with a loss of -1.3 dB resulting in 90 mW average power.

3. Pulse characterization

Pulse spectra were measured before and after the PCF to characterize the effect of the self-phase modulation. The pulse spectrum shows power-dependent broadening after the PCF in Fig. 2(b), as would be expected in the case of self-phase modulation.

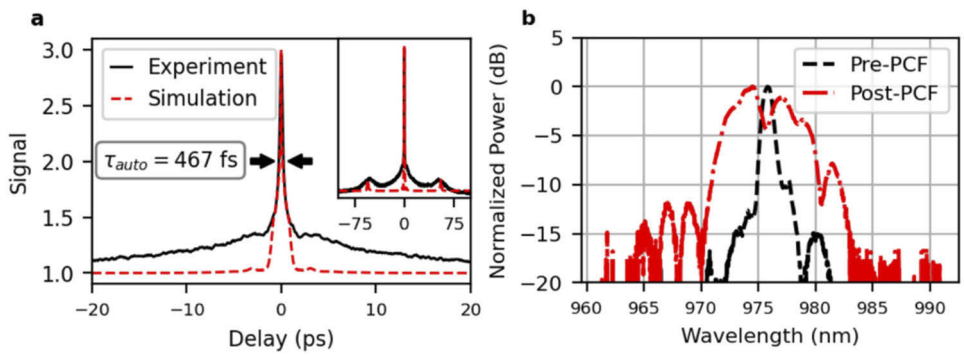

Fig. 2. **a** Autocorrelation of the output pulses and the autocorrelation of a simulated pulse from the system. Experiment autocorrelation full-width at half-max is labeled. Insert shows full extent of pulse, from autocorrelation peak to background levels. **b** Laser spectra before and after photonic crystal fiber (PCF), showing spectral broadening from self-phase modulation.

Intensity autocorrelations used to characterize the pulse are shown in Fig. 2(a). The autocorrelation shows a central peak with a width of 467 fs with a pedestal extending from the base of the peak. A side pulse is seen at 50 ps from the center, corresponding to the 18 GHz amplitude modulation. The pedestal is caused by two effects. The first is uncompressed nonlinear phase from the self-phase modulation in the photonic crystal fiber [36–38]. The second is incoherent artifacts from the uncorrelated spectral phase of the gain-switched seed [39]. This jitter brings the modulation away from the ideal, purely quadratic modulation of a perfect time lens pulse.

The intensity autocorrelation alone does not provide a determination of the electric field, but supports that the laser pulses are ps-scale with peak power in the kW range when viewed with the imaging results from Section 4. Uncompressed nonlinear phase, timing jitter in the seed pulses (~10 ps) [40], and the strength of phase modulation from the electro-optical modulator, limit the achievable pulse width. Pulse power is limited by the losses in the cladding mode stripper, PCF coupling, and grating compressor (total ~-3.5 dB) as well as gain saturation of Yb fiber amplification at 976 nm, most of which can be improved by removing free space losses. If greater pulse energies are desired, the repetition rate may be reduced electronically, although dispersion compensation would need to be adjusted for the increase in self-phase modulation from increased power [21].

4. Two photon microscopy demonstration

To prove our system is viable for use in two photon microscopy and can achieve results comparable to Ti:sapphire lasers in terms of tissue penetration depth, the system was integrated with a two-photon microscope. Imaging of eGFP-labeled oligodendrocytes was chosen for a demonstration

Biomedical Optics EXPRESS

as the potential size and cost reduction our system offers is well suited to expanding recording of neural activity of freely moving animals in real time. Our microscope (Fig. 1(b)) consists of a galvanometer mirror system which sends the pulses through a scan and tube lens system. A dichroic is placed before the objective and filters out the fluorescence signal which is sent to a photo-multiplier tube (PMT). The sample is mounted above the objective on a z-axis stepper motor for axial scanning. A dichroic mirror (Semrock FF740-Di01) and notch filters (Thorlabs MF525-39, Chroma ET520/20 m) provide ~90 dB of excitation source isolation to the PMT. During image collection, incident power was controlled using a half-wave plate mounted on a piezo rotation stage and a polarizer.

A 1 mm thick, coronal slice of fixed, PLP-eGFP mouse brain tissue was mounted on a microscope slide in VECTASHIELD Plus Antifade Mounting Media (H-1900). All animal procedures were performed in accordance with protocols approved by the Institutional Animal Care and Use Committee of the University of Colorado Anschutz Medical Campus. The neo-cortex region of the sample was imaged using a water immersion microscope objective (Olympus, 20x 1 NA, XLUMPLFLN20XW). An average power of 28 mW (maximum used at depth) was measured at the back aperture of the objective during tissue imaging. The spot size calculated on the focal plane was 600 nm with a 1.6 µm depth of focus. To collect a volumetric image, samples were scanned with a 260×260 µm^2 field of view going from top to bottom in 5 µm steps with power and pixel dwell time increased with imaging depth into the sample. For the first layers, pixel dwell time was 24 µs for the images (400×400 pixels) for a total acquisition time of 3.9 seconds per frame. For depths greater than 800 µm, the dwell time was 64 µs for a total time of 11 seconds per frame. This acquisition time is over twice as fast than previous time lens systems for similar samples and penetration depths [21]. Sample bleaching was not observed

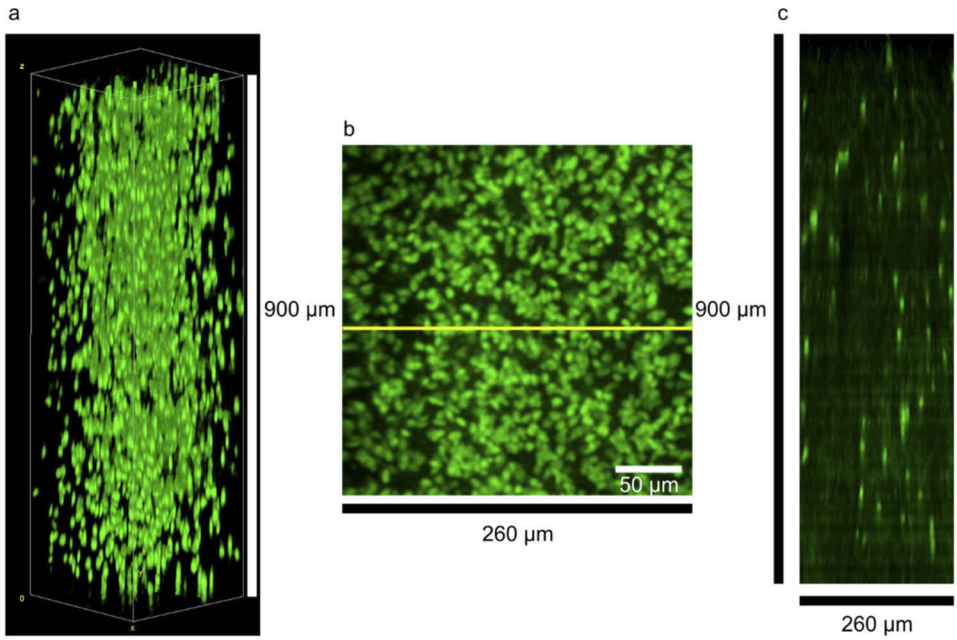

Fig. 3. Deep tissue, two-photon microscope images of oligodendrocyte cell bodies in the neocortex region of fixed, PLP-eGFP mouse brain slices. Images were acquired at 5-micron intervals in the z direction for 900 microns. **a** 3D stack of the slices (see Visualization 1). **b** Projection in the z direction (maximum intensity). **c** Slice through the image stacks with the slice position denoted by the yellow line in **b**.

Biomedical Optics EXPRESS

after this acquisition. Resulting volume images for a depth of 900 μm are shown in Fig. 3 with a projection and vertical slice (see Visualization 1). The decreased resolution in the z-axis is expected as the laser is focused at greater depths through index of refraction heterogeneities in the tissue itself and between the tissue sample and the mounting media, as these aberrations were not measured or corrected in the system [7,11]. Higher resolution images (1024 × 1024 pixels) were acquired at 100 μm steps with a selection shown in Fig. 4 to emphasize fine details in the sample. Individual soma and processes are resolvable, even at depths of 900 μm into the sample, and imaging depth is only limited by the thickness of the sample. Although the signal to noise ratio is limited by peak power and repetition rate in comparison to a Ti:Sapphire, images taken at depth in tissue are comparable to those acquired with a Ti:Sapphire system (Fig. S2) and clearly demonstrate our system's utility for multiphoton microscopy.

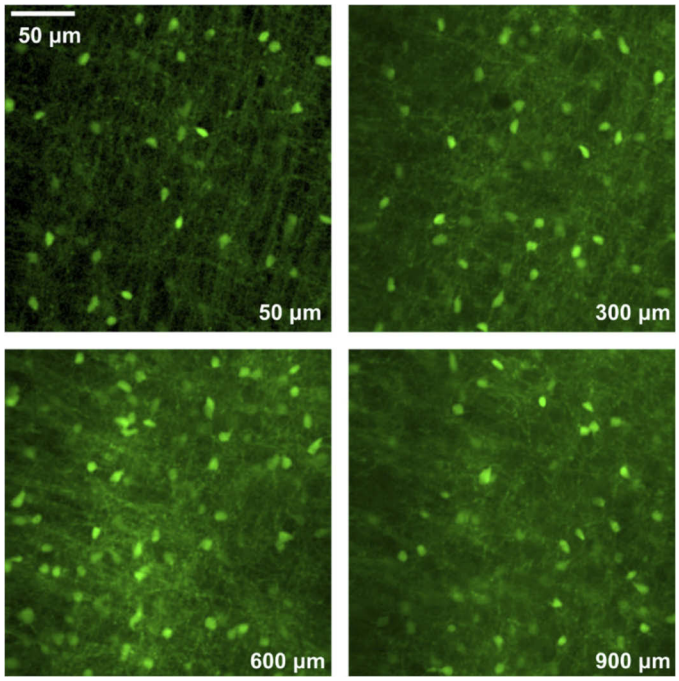

Fig. 4. Two-photon microscope images of oligodendrocyte cell bodies and processes in the neocortex region of fixed, PLP-eGFP mouse brain slices. These images were taken at a selection of depths into a 1 mm thick coronal slice of brain tissue and have their depths denoted in the lower left corners.

5. Conclusion

We have demonstrated a 976 nm diode-based laser source with ps-scale pulses and kW class peak power suitable for two-photon microscopy based on time-lens pulse generation and pulse compression. Our system was successfully utilized for two-photon microscopic imaging of eGFP labeled mouse oligodendrocytes at depths up to 900 μm.

When looking towards the future of multiphoton microscopy, it is clear that new laser sources in the near-IR are required to expand research applications and for eventual commercial and medical use. Diode-based designs create a clear path forward for reduction in size and cost and lends itself to robust operation in a variety of environments. Our design validates the feasibility of a compact two photon laser microscopy source with these benefits which will increase access to and widen the application off multiphoton microscopy in research and clinical settings.

Biomedical Optics EXPRESS

Funding. National Institute of Neurological Disorders and Stroke (1R01NS118188); State of Colorado Advanced Industry Accelerator (CTGG1 2017-1874); National Institutes of Health SPARC (1OT2OD023852).

Acknowledgements. The authors would like to thank Professor Diego Restrepo and Gabriel Martinez for supplying the samples for imaging. Thanks also goes to Megan Kelleher for assistance with the laser system and Dr. Scott Diddams and Gabriel Ycas for technical discussions. The content of this publication is solely the responsibility of the authors and does not necessarily represent the official views of the National Institutes of Health.

Disclosures. The authors declare no conflicts of interest.

Data availability. Data presented in this paper may be obtained from the authors upon reasonable request.

Supplemental document. See Supplement 1 for supporting content.

References

1. B. N. Ozbay, G. L. Futia, M. Ma, V. M. Bright, J. T. Gopinath, E. G. Hughes, D. Restrepo, and E. A. Gibson, "Three dimensional two-photon brain imaging in freely moving mice using a miniature fiber coupled microscope with active axial-scanning," Sci. Rep. **8**(1), 8108–8114 (2018).
2. M. R. Warden, J. A. Cardin, and K. Deisseroth, "Optical Neural Interfaces," Annu. Rev. Biomed. Eng. **16**(1), 103–129 (2014).
3. V. Sriramoju and R. R. Alfano, "*In vivo* studies of ultrafast near-infrared laser tissue bonding and wound healing," J. Biomed. Opt. **20**(10), 108001 (2015).
4. A. Burgess, T. Nhan, C. Moffatt, A. L. Klibanov, and K. Hynynen, "Analysis of focused ultrasound-induced blood-brain barrier permeability in a mouse model of Alzheimer's disease using two-photon microscopy," J. Controlled Release **192**, 243–248 (2014).
5. S. Liebscher and M. Meyer-Luehmann, "A peephole into the brain: Neuropathological features of Alzheimer's disease revealed by in vivo two-photon imaging," Front. Psychiatry **3**, 1–11 (2012).
6. L. Li, C.-W. Zhang, G. Y. J. Chen, B. Zhu, C. Chai, Q.-H. Xu, E.-K. Tan, Q. Zhu, K.-L. Lim, and S. Q. Yao, "A sensitive two-photon probe to selectively detect monoamine oxidase B activity in Parkinson's disease models," Nat. Commun. **5**(1), 3276 (2014).
7. F. Helmchen and W. Denk, "Deep tissue two-photon microscopy," Nat. Methods **2**(12), 932–940 (2005).
8. K. Svoboda and R. Yasuda, "Principles of two-photon excitation microscopy and its applications to neuroscience," Neuron **50**(6), 823–839 (2006).
9. P. Theer, M. T. Hasan, and W. Denk, "Two-photon imaging to a depth of 1000 µm in living brains by use of a Ti:Al_2O_3 regenerative amplifier," Opt. Lett. **28**(12), 1022 (2003).
10. E. E. Hoover and J. A. Squier, "Advances in multiphoton microscopy technology," Nat. Photonics **7**(2), 93–101 (2013).
11. W. R. Zipfel, R. M. Williams, and W. W. Webb, "Nonlinear magic: multiphoton microscopy in the biosciences," Nat. Biotechnol. **21**(11), 1369–1377 (2003).
12. T. Hellerer, C. Polzer, A. Friedenauer, I. Greisberger, B. Wolfring, and C. Skrobol, "920 nm fiber laser delivering 100 fs pulses for nonlinear microscopy," in *Multiphoton Microscopy in the Biomedical Sciences XIX*, A. Periasamy, P. T. So, and K. König, eds. (SPIE, 2019), p. 29.
13. J. Lhermite, C. Lecaplain, G. Machinet, R. Royon, A. Hideur, and E. Cormier, "Mode-locked 05 µJ fiber laser at 976 nm," Opt. Lett. **36**(19), 3819 (2011).
14. C. Lefort, "Laser sources in multiphoton microscopy: overview and optimization," in *Unconventional Optical Imaging*, C. Fournier, M. P. Georges, and G. Popescu, eds. (SPIE, 2018), p. 30.
15. S. Kono, H. Watanabe, R. Koda, N. Fuutagawa, and H. Narui, "140-fs duration and 60-W peak power blue-violet optical pulses generated by a dispersion-compensated GaInN mode-locked semiconductor laser diode using a nonlinear pulse compressor," Opt. Express **23**(25), 31766 (2015).
16. F. R. Ahmad, Y. W. Tseng, M. A. Kats, and F. Rana, "Energy limits imposed by two-photon absorption for pulse amplification in high-power semiconductor optical amplifiers," Opt. Lett. **33**(10), 1041 (2008).
17. A. Galvanauskas, P. Blixt, and J. A. Tellefsen, "Generation of femtosecond optical pulses with nanojoule energy from a diode laser and fiber based system," Appl. Phys. Lett. **63**(13), 1742–1744 (1993).
18. J. T. Gopinath, B. Chann, R. K. Huang, C. Harris, J. J. Plant, L. Missaggia, J. P. Donnelly, P. W. Juodawlkis, and D. J. Ripin, "980-nm monolithic passively mode-locked diode lasers With 62 pJ of pulse energy," IEEE Photonics Technol. Lett. **19**(12), 937–939 (2007).
19. J. J. Plant, J. T. Gopinath, B. Chann, D. J. Ripin, R. K. Huang, and P. W. Juodawlkis, "250 mW, 15 µm monolithic passively mode-locked slab-coupled optical waveguide laser," Opt. Lett. **31**(2), 223 (2006).
20. B. H. Kolner and M. Nazarathy, "Temporal imaging with a time lens," Opt. Lett. **14**(12), 630 (1989).
21. R. D. Niederriter, B. N. Ozbay, G. L. Futia, E. A. Gibson, and J. T. Gopinath, "Compact diode laser source for multiphoton biological imaging," Biomed. Opt. Express **8**(1), 315 (2017).
22. D. Strickland and G. Mourou, "Compression of amplified chirped optical pulses," Opt. Commun. **56**(3), 219–221 (1985).
23. W. J. Tomlinson, R. H. Stolen, and C. V. Shank, "Compression of optical pulses chirped by self-phase modulation in fibers," J. Opt. Soc. Am. B **1**(2), 139–149 (1984).

Biomedical Optics EXPRESS

24. K. Wang and C. Xu, "Wavelength-tunable high-energy soliton pulse generation from a large-mode-area fiber pumped by a time-lens source," Opt. Lett. **36**(6), 942 (2011).
25. W. Fu, L. G. Wright, and F. W. Wise, "High-power femtosecond pulses without a modelocked laser," Optica **4**(7), 831 (2017).
26. J. van Howe, J. H. Lee, and C. Xu, "Generation of 35 nJ femtosecond pulses from a continuous-wave laser without mode locking," Opt. Lett. **32**(11), 1408 (2007).
27. C. Xu and W. R. Zipfel, "Multiphoton excitation of fluorescent probes," Cold Spring Harb. Protoc. **2015**(3), pdb.top086116 (2015).
28. C. L. Evans and X. S. Xie, "Coherent anti-Stokes Raman scattering microscopy: chemical imaging for biology and medicine," Annu. Rev. Anal. Chem. **1**(1), 883–909 (2008).
29. H. Hajjar, H. Boukhaddaoui, A. Rizgui, C. Sar, J. Berthelot, C. Perrin-Tricaud, H. Rigneault, and N. Tricaud, "Label-free non-linear microscopy to measure myelin outcome in a rodent model of Charcot-Marie-Tooth diseases," J. Biophotonics **11**(12), e201800186 (2018).
30. B. S. Mallon, H. E. Shick, G. J. Kidd, and W. B. Macklin, "Proteolipid promoter activity distinguishes two populations of NG2-positive cells throughout neonatal cortical development," J. Neurosci. **22**(3), 876–885 (2002).
31. J. K. O'Daniel and M. Achtenhagen, "High-power spectrally-stable DBR semiconductor lasers designed for pulsing in the nanosecond regime," in *Novel In-Plane Semiconductor Lasers IX*, A. A. Belyanin and P. M. Smowton, eds. (2010), Vol. 7616, p. 76160W.
32. B. Resan, R. Aviles-Espinosa, S. Kurmulis, J. Licea-Rodriguez, F. Brunner, A. Rohrbacher, D. Artigas, P. Loza-Alvarez, and K. J. Weingarten, "Two-photon fluorescence imaging with 30 fs laser system tunable around 1 micron," Opt. Express **22**(13), 16456 (2014).
33. S. Mirkhanov, A. H. Quarterman, C. J. C. P. Smyth, B. B. Praveen, P. Appleton, C. Thomson, S. Swift, and K. G. Wilcox, "Optimal repetition rate and pulse duration studies for two photon imaging," in *Multiphoton Microscopy in the Biomedical Sciences XVII*, A. Periasamy, P. T. C. So, K. König, and X. S. Xie, eds. (2017), Vol. 10069, p. 100692F.
34. F. Roeser, C. Jauregui, J. Limpert, and A. Tünnermann, "94 W 980 nm high brightness Yb-doped fiber laser," Opt. Express **16**(22), 17310 (2008).
35. J. Wu, X. Zhu, H. Wei, K. Wiersma, M. Li, J. Zong, A. Chavez-Pirson, V. Temyanko, L. J. LaComb, R. A. Norwood, and N. Peyghambarian, "Power scalable 10 W 976 nm single-frequency linearly polarized laser source," Opt. Lett. **43**(4), 951 (2018).
36. J. P. Heritage, R. N. Thurston, W. J. Tomlinson, A. M. Weiner, and R. H. Stolen, "Spectral windowing of frequency-modulated optical pulses in a grating compressor," Appl. Phys. Lett. **47**(2), 87–89 (1985).
37. R. Thurston, J. Heritage, A. Weiner, and W. Tomlinson, "Analysis of picosecond pulse shape synthesis by spectral masking in a grating pulse compressor," IEEE J. Quantum Electron. **22**(5), 682–696 (1986).
38. E. M. Dianov, L. M. Ivanov, P. V. Mamyshev, and A. M. Prokhorov, "Efficient compression of high-energy laser pulses," IEEE J. Quantum Electron. **25**(4), 828–835 (1989).
39. J. Ratner, G. Steinmeyer, T. C. Wong, R. Bartels, and R. Trebino, "Coherent artifact in modern pulse measurements," Opt. Lett. **37**(14), 2874 (2012).
40. "T165 picosecond to nanosecond laser diode pulser," https://www.highlandtechnology.com/DSS/T165DS.shtml.